J. Sens. Sens. Syst., 4, 271–280, 2015
www.j-sens-sens-syst.net/4/271/2015/
doi:10.5194/jsss-4-271-2015

JSSS Journal of Sensors and Sensor Systems Open Access

Investigating the influence of Al-doping and background humidity on NO_2 sensing characteristics of magnetron-sputtered SnO_2 sensors

A. A. Haidry[1], **N. Kind**[1,a], **and B. Saruhan**[1]

[1]Institute of Materials Research, German Aerospace Center (DLR) Linder Hoehe, 51147 Cologne, Germany
[a]currently at: Laboratoire de Tribologie et Dynamique des Systèmes (LTDS) – UMR 5513 Bâtiment D4 Ecole Centrale de Lyon 36 Avenue Guy DE COLLONGUE 69134 Ecull, France

Correspondence to: A. A. Haidry (azhar.haidry@dlr.de) and B. Saruhan (bilge.saruhan@dlr.de)

Received: 14 January 2015 – Revised: 13 July 2015 – Accepted: 24 July 2015 – Published: 31 August 2015

Abstract. Elevated temperatures and humidity contents affect response, lifetime and stability of metal-oxide gas sensors. Remarkable efforts are being made to improve the sensing characteristics of metal-oxide-based sensors operating under such conditions. Having versatile semiconducting properties, SnO_2 is prominently used for gas sensing applications. The aim of the present work is to demonstrate the capability of the Al-doped SnO_2 layer as NO_2 selective gas sensor working at high temperatures under the presence of humidity. Undoped SnO_2 and Al-doped SnO_2 (3 at. % Al) layers were prepared by the radio frequency (r.f.) reactive magnetron sputtering technique, having an average thickness of 2.5 µm. The sensor response of Al-doped SnO_2 samples was reduced in the presence of background synthetic air. Moreover, under dry argon conditions, Al doping contributes to obtain a stable signal and to lower cross-sensitivity to CO in the gas mixtures of $CO + NO_2$ at temperatures of 500 and 600 °C. The Al-doped SnO_2 sensors exhibit excellent chemical stability and sensitivity towards NO_2 gas at the temperature range of 400–600 °C under a humid environment. The sensors also showed satisfactory response ($\tau_{res} = 1.73$ min) and recovery ($\tau_{rec} = 2.7$ min) towards 50 ppm NO_2 in the presence of 10 % RH at 600 °C.

1 Introduction

Semiconducting metal oxides (MOX) are the dominant material in the gas sensor industry with SnO_2 being a widely employed material for various emission gases (Göpel and Schmierbaum, 1995; Yamazoe and Shimanoe, 2007; Tricoli et al., 2010; Bochenkov et al., 2010). However, its use is limited to low operating temperatures in the range of 150–350 °C, because of low stability and poor selectivity obtained at higher temperatures (Yamazoe and Shimanoe, 2007; Tricoli et al., 2010). Among other MOX sensors, SnO_2 is widely studied as it is sensitive to many gases. Many metal additives, such as Pt, Pd, Ag and Au, have been used to improve the SnO_2 sensing properties (Göpel and Schmierbaum, 1995; Bochenkov et al., 2010). In the case of Al doping, Al-doped SnO_2 thin sensor films were produced by sputtering Sn on the substrate and using rheotaxial growth and a thermal oxidation process (Faglia et al., 1996). It has been reported that Al-doped SnO_2 sensor layers show better sensitivity to NO_2 when the voltage is swept from direct current (DC) to 4 MHz at impedance measurements (Faglia et al. 1994).

It is well known that operating conditions of a sensor play a significant role in defining the sensor properties such as sensitivity, response/recovery time, stability, selectivity, etc. (Pavelko et al., 2010). While the effect of background water and oxygen species on gas sensing properties of SnO_2 materials has recently been reported (Korotcenkov et al., 2007; Großmann et al., 2013), this issue is still a subject of debate due to the complexity of this matter. A significant decrease in sensor response has been reported when the SnO_2 layer was exposed to a reducing gas (CO) in the presence of humidity, possibly due to pre-adsorbed oxygen being the only available ions for both CO and humidity (Großmann et al., 2013). Moreover, an increase in the CO sensing was reported in the

presence of dry air, relying on the availability of more surface oxygen adsorbed from the air. Molecular water and oxygen species are adsorbed on the sensor surface below 150 °C under atmospheric pressure, while at higher temperatures (e.g., above 250 °C for water and 150 °C for oxygen) the hydroxyl groups and ionic oxygen are reported to be present on the sensor surface (Batzill et al., 2006). These reports indicate that the role of background oxygen and water in sensing can be significant at a wider temperature range, especially for application areas where the presence of these species cannot be ruled out.

In this report, we demonstrate the effect of aluminium doping on NO_2 sensing of SnO_2 sensors at relatively higher temperatures (> 400 °C) and analyze the effect of humidity on NO_2 sensing. The sensor coatings were prepared by means of a radio frequency (r.f.) reactive magnetron sputtering technique on alumina-based sensor platforms decorated with platinum inter-digital electrodes. The sensors were subsequently annealed at 800 °C to achieve a crystalline structure. The sensitivity of the undoped and Al-doped SnO_2 coatings for NO_2 in dry as well as in humid argon at working temperatures $T_w = 400$–600 °C are presented. The sputtering technique allows for flexibility in adjusting composition and layer thickness yielding fine columnar structured morphology. Doping of SnO_2 with inexpensive aluminum and its deposition by sputtering on simple, designed sensor platforms will yield sensors competing with sophisticated and expensive nanowire/nanotube sensor layers. This paper aims at the validation of this concept.

2 Experimental

2.1 Preparation of sensing layers

The sensing layers were deposited by means of r.f. magnetron reactive sputtering on sensor platforms of 4.2 mm × 24.5 mm dimension. These sensor platforms were of Al_2O_3 substrates which contained inter-digital platinum electrodes (IDEs) previously patterned with screen printing methods, (see Fig. 1a). Each IDEs circuit contains five parallel 300 µm wide fingers with a 300 µm gap between two successive electrodes. The thickness of screen-printed Pt is about 2 µm. The sputter equipment (from Co. von Ardenne Anlagentechnik GmbH, Germany) can contain two metallic or ceramic targets. In the present case, Sn and Al metallic targets of same diameter ($\varnothing = 90$ mm) were used and placed opposite to each other. Both targets were adjusted with different applied powers (P_{Sn}, P_{Al}). The sputtering process was carried out without any substrate heating and under high purity Argon + O_2 gaseous mixture (purity of Argon and O_2 were 99.9990 % and 99.9995 %, respectively). The partial pressures of oxygen (p_{O_2}) and argon (p_{Ar}) were controlled by mass flow controllers from MKS Instruments GmbH. During the deposition of undoped SnO_2 coatings, no rotation of substrate holders was applied. During the coating process of Al-doped SnO_2, hereafter denoted as $SnO_2 : Al$, the substrates were rotated at a rate of 13 rpm. This rotation is necessary to achieve homogenous distribution of aluminium in the SnO_2 matrix. The sputtering conditions for both types of sensing layers are listed in Table 1. Under the given sputtering conditions, sensing layers of thickness of approximately 2.5 µm were obtained. Both sensor types (i.e., undoped SnO_2 and $SnO_2 : Al$) were manufactured during three different coating runs having 4–6 sensor platforms. At least three of these sensors were tested for their sensing properties.

Single crystal Al_2O_3 sapphire circular disks ($\varnothing = 13$ mm) and silicon (Si) substrates (20 × 20 mm) were also placed side by side to the sensor platforms during each deposition run to be used for XRD (X-ray diffraction) measurements and EDX (energy dispersive X-ray) analysis, respectively, in order to avoid Pt interference from the inter-digital circuitry and Al from Al_2O_3 substrates. After deposition, the layers are annealed in static air at 800 °C for 3 h with a heating rate of 100 °C 15 min^{-1} in a M110 muffle furnace from Heraeus instruments. This ex situ annealing is necessary to obtain crystalline structures and also to stabilize the morphology and phase conditions prior to high temperature sensor tests.

2.2 Structural, morphological and compositional characterization

The structural investigation of the sensors was performed in Bragg–Brantano geometry by the XRD method, using s Siemens D5000 X-ray diffractometer with a CuKα radiation ($\lambda_{CuK\alpha} = 0.15418$ nm) and the graphite-curved monochromator. For phase analysis, $\theta/2\theta$- spectra is measured with an acceleration voltage of 40 kV at a step of 0.020° and a step rate of 3 s $step^{-1}$. The obtained data were compared with the JCPS database (Joint Committee on Powder Diffraction Standards) via EVA software from Bruker AXS in the range of 10–80° . The analysis of microstructure, surface morphology and chemical composition was carried out by using a field emission scanning electron microscope (FE-SEM, Carl Zeiss NTS Ultra 55) equipped with an EDX spectrometer.

2.3 Gas sensing characterization

Gas sensing characterization was carried out in a computer-controlled gas sensing experimental setup. This sensor and catalyst characterization unit (SESAM) consists of an eight-channel flow controller from MKS Instruments GmbH (MFC-647b) followed by a gas mixing chamber consisting of a CARBOLITE tube furnace with a quartz-glass recipient and DC-measurement unit from a Keithley 2635A Sourcemeter. The sample was mounted on a sample holder and then placed in a quartz-glass recipient with no heater at the back of the sensor sample. This setup allows us to accurately measure resistance R up to 10 GΩ at various

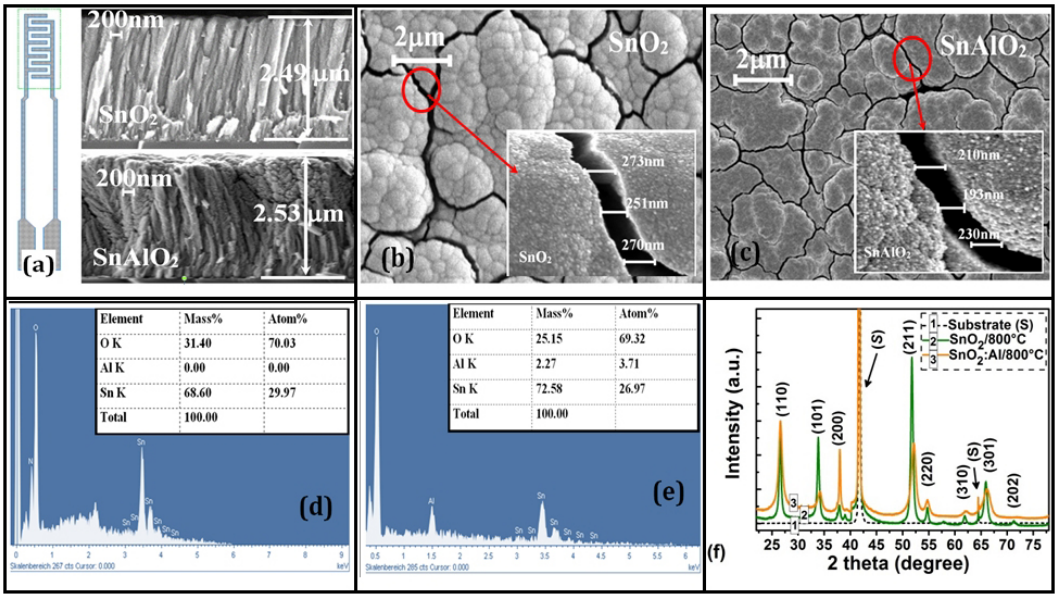

Figure 1. Structural and morphological characteristics of the sensing layers. **(a)** Schematic of Al_2O_3 sensor platforms with inter-digital electrodes (IDEs) and FE-SEM micrographs of both layers at the cross section confirming the columnar structure. **(b)** and **(c)** FE-SEM micrographs of SnO_2 and SnO_2 : Al layers, respectively, showing grain size differences and the insets showing the cracks generated during annealing. **(d)** and **(e)** EDX spectra of SnO_2 and SnO_2 : Al layers, respectively. **(f)** The X-ray diffractograms of c-cut single crystal sapphire Al_2O_3 substrate (1), SnO_2 (2) and SnO_2 : Al (3). The sensing layers were ex situ annealed at a temperature of 800 °C in static air, the peak from (0006) the plane of c-cut sapphire Al_2O_3 is denoted as "S".

Table 1. Deposition conditions for the undoped and Al-doped SnO_2 coatings.

Layer	$p_{chamber}$ (bar)	p_{O_2} (sccm)	p_{Ar} (sccm)	P_{Sn} (W)	P_{Al}(W)	Sputter time (h)	Layer thickness (µm)
SnO_2	6.10×10^{-3}	45	70	100	0	3	2.49
SnO_2 : Al	5.3×10^{-3}	35	70	70	150	12.50	2.53

gas concentrations and various operating temperatures up to 1200 °C. Sensor tests in SESAM are carried out in a quartz-glass recipient heated by a tube furnace, the temperature of which is controlled over three cascades and adjusted by a thermocouple positioned in the quartz recipient at a distance of 2 cm from the sensor surface. The quartz-glass recipient has a 3 m long spiral through which the test gas is sent and heated by the same furnace in order to avoid cooler gas contacting the sensor surface. The whole system including the gas inlet and sensor chamber is kept heated during the sensor test. Relying on the longer soaking times before and during the gas exposure (e.g., 30–60 min), the expected temperature difference between the thermocouple and the sensor surface will be negligibly small. Prior to gas-sensing measurements, a warm-up heating at the required testing temperature (i.e., 400–600 °C) was employed to all samples for 1 h under argon flow. This heating is necessary (Kim et al., 2013) to achieve electrical and chemical equilibrium at the sample surface. During the warming-up period, adsorption and desorption of gas molecules results in chemical stabilization of the sensor surface and a steady baseline resistance is obtained.

All measurements were done in argon flow at a rate of 400 mL min^{-1} with a constant current of 1×10^{-6} A. Considering the ideal cases, the gas mixing process in the chamber is governed by the differential equation as given in Haidry et al. (2011). The gas mixing time τ_{mix} can be estimated as the chamber volume divided by the flow rate. The volume of the cylindrical chamber for pre-mixing the gases is 110 cm^3 and the flow rate is 400 mL min^{-1}, which gives a mixing time constant of 16.2 s. Further delay of a few seconds must be added to residence time as the gas mixture flows through approximately 4.5 m long tubes of 4.0 mm diameter before entering the sensing chamber. For calculation of the reaction/recovery times, this delay has been taken into account. The NO_2 concentrations were varied in the range of 50–200 ppm in dry and humid (1–10 % RH) argon (purity $\geq$ 99.998 %) for a continuous cycle of 30 min.

3 Results and discussion

3.1 FE-SEM and EDX analysis

As the cross-sectional micrographs of undoped and Al-doped SnO_2 in Fig. 1a show, the morphologies of both layers are very similar and columnar, despite the fact that the SnO_2 : Al layer was rotated during deposition. As mentioned earlier, the purpose of rotation was to obtain a uniform Al distribution in Sn bulk. The columnar structure and layer thicknesses of about 2.5 µm were checked using cross sections by SEM and presented in Fig. 1a. The top-view SEM micrograph of the SnO_2 layer deposited on sensor platforms (Fig. 1b) indicates fine columns leading to dense layer morphology with relatively wide cracks. The surface micrograph of the heat-treated layer does not exhibit any granular structure and XRD results confirm this (see Sect. 3.2 below). For SnO_2 : Al layers, the top-view SEM micrograph confirms the presence of more finer columns (i.e., grains) with a denser morphology and narrow cracks (Fig. 1c). The chemical composition of the SnO_2 is found to be 1 : 2, while the average Al^{3+} contents lie at about 3 at. % as confirmed by the EDX analysis (Fig. 1d, e).

3.2 XRD analysis

The XRD diffractograms of sapphire substrate without any layer, SnO_2 and SnO_2 : Al are shown in Fig. 1f. The XRD patterns of the both sensing layers, i.e., SnO_2 and SnO_2 : Al, are found to be normalized with a peak from (0006) the plane of c-cut sapphire Al_2O_3 at $2\theta = 41.7°$. After annealing, the polycrystalline sensing layers exhibit an orientation along (110), (101), (200), (211), (220), (310), and (301) at $2\theta = 26.6$, 33.9, 37.9, 51.8, 54.7, 61.9 and 65.9°, respectively. These values are given in Table 2. These peaks are those which have three extra-low-intensity peaks at $2\theta =$ 38.9, 57.8, and 71.8° at the undoped SnO_2 sensing layers. The strong-intensity peak for SnO_2 (211) corresponds to $2\theta = 37.9°$ and for SnO_2 : Al (200) to $2\theta = 37.9°$. Although SnO_2 shows good lattice match with the Al_2O_3 substrate, a slight shift of $2\theta = \pm 0.02°$ can be observed comparing the above listed peaks with the standard XRD powder diffraction file (PDF2 #00-041-1445) of tetragonal SnO_2. According to Bazargan et al. (2013), this shift is most probably caused due to the difference in surface structure of rhombus Al_2O_3 and tetragonal SnO_2/SnO_2 : Al layers. No extra peak(s) for Al or its oxides are observed. Based on similar results (Gürakar et al., 2014), the authors conclude that no extra Al peaks in the XRD diffractogram can be observed, indicating a homogenous distribution of Al atoms within the SnO_2 matrix. Moreover, they report that intensities decrease significantly and the peaks are broadened. This may possibly be caused by the replacement of Sn^{4+} ions by Al^{3+} ions, as already mentioned in Mohagheghi and Saremi (2004). The average grain size of SnO_2 : Al layers (12 nm) is smaller than that of SnO_2 (45 nm); the grain size was estimated by means of the Scherrer formula.

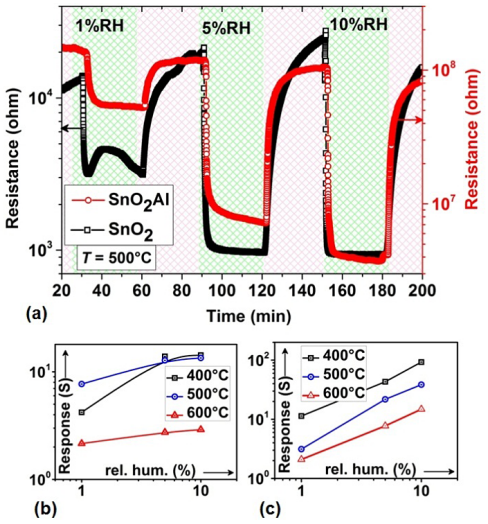

Figure 2. **(a)** The dynamic responses of SnO_2 (□) and SnO_2 : Al (◯) layers towards 1–10 % RH at $T_w = 500$, **(b)** response versus relative humidity correlation of SnO_2 and **(c)** SnO_2 : Al. The response was recorded for a cyclic exposure of 30 min to dry and humid argon.

3.3 Humidity sensing properties

Dynamic testing of both types of sensors under relative humidity (RH) is performed in the temperature range of 400–600 °C in order to understand the chemistry involved in NO_2 sensing under a humid environment. Both sensing layers show reproducible dynamic responses (Fig. 2), where the resistance of the layers decrease on exposure to various RH. This decrease is linear in the relative humidity range of 1–10 % RH as shown in Fig. 3b. The response (τ_{res}) and recovery (τ_{rec}) times are estimated for the 90 % change of the final saturated sensor resistance when switching the gas ON and OFF. The response ($S_{\%RH} = R_{argon}/R_{\%RH}$) and response times for the undoped SnO_2 layers are better at $T_w = 500$ °C ($\tau_{res} = 1.2$, 1.5 and 1.9 min towards 1, 5 and 10 % RH, respectively). However, as given in Table 3, longer recovery times are recorded reaching to several tens of minutes ($\tau_{rec} =$ 24–30 min at $T_w = 400$ °C and $\tau_{rec} = 6.6$, 13.9 and 24.8 min towards 1, 5 and 10 % RH, respectively, at $T_w = 500$ °C). On the other hand, the increase of temperature to $T_w = 600$ °C yields relatively shorter recovery times ($\tau_{rec} = 2.9$, 3.1 and 5.5 min towards 1, 5 and 10 % RH).

Interestingly, the Al doping of SnO_2 results in more stable and reproducible sensing characteristics towards various RH (Fig. 2a). The response times are somewhat in the same range as those of undoped SnO_2 at $T_w = 400$ °C and become shorter with further increase of the working temperature, i.e., at $T_w = 500$ and 600 °C. Meanwhile, a significant shortening

Table 2. XRD-obtained peaks and orientations, where hkl are the Miller indices. The cells with × indicate NO peak observed at given 2θ.

Layer	2θ°/hkl	2θ°/hkl	2θ°/hkl	2θ°/hkl	2θ°/hkl	2θ°/hkl	2θ°/hkl	2θ°/hkl	2θ°/hkl	2θ°/hkl
SnO_2	26.6/(110)	33.9/(101)	37.9/(200)	38.9/(111)	51.8/(211)	54.7/(220)	57.8/(002)	61.9/(310)	65.9/(301)	71.8/(320)
SnO_2 : Al	26.6/(110)	33.9/(101)	37.9/(200)	×	51.8/(211)	54.7/(220)	×	61.9/(310)	65.9/(301)	×

Table 3. Comparison of recovery times for SnO_2 and SnO_2 : Al sensing layer towards 1, 5 and 10 % RH (without NO_2 exposure).

T_w (°C)	400			500			600		
Humidity (%)	1 %	5 %	10 %	1 %	5 %	10 %	1 %	5 %	10 %
τ_{rec} (min) for SnO_2	24.30	26.5	30	6.65	13.9	24.8	2.95	3.16	5.55
τ_{rec} (min) for SnO_2 : Al	4.68	8.9	12	5.83	5.11	3.85	4.03	2.11	2.23

of recovery time is recorded at each working temperature; see Table 3. The response to increasing humidity concentrations (% RH) shows the similar decreasing trend (Fig. 2b, c) with increasing temperature (T_w) as that with undoped SnO_2 layers (see Table 3). The reaction and recovery time constants in most cases can be correlated to operating temperature, as sensors produce different sensing properties depending on the operating conditions (Chen and Lu, 2005). It is observed in Fig. 2 that sensitivity and sensor response towards humidity is improved by Al doping. The response of the undoped SnO_2 layer towards lower humidity concentrations (e.g., 1 % RH) is very unsteady and recovery is very slow.

3.4 NO_2 sensing properties

The dynamic responses of SnO_2 and SnO_2 : Al sensors towards various NO_2 gas concentrations (50, 100 and 200 ppm) in dry argon background were recorded at $T_w = 400$, 500 and 600 °C; see Fig. 3. We define the sensor response/signal to NO_2 by the following equation: $S_{NO_2} = R_{NO_2}/R_{argon}$. A decrease in the sensor response of SnO_2 layers with increase in T_w was observed with incomplete baseline recovery at $T_w = 400$–500 °C, which causes a drift in sensor signal (Fig. 3a). Similar observations were reported in a previous study (Barsan et al., 2007), where decrease in sensitivity and short-term stability of SnO_2 was recorded when temperature increased above $T_w = 350$ °C. In contrast, as seen in Fig. 3b, SnO_2 : Al layers show a stable and reproducible response at $T_w = 600$ °C with reasonable recovery, although a weak or no response is obvious at $T_w = 400$ and 500 °C. These results indicate that Al doping leads to better short-term stability and sensitivity at 600 °C. The short-term stability means the ability of a sensor to produce the same dynamic response and to reach the same baseline resistance after switching OFF the gas; this also means a reproducible sensor response. The long-term stability defines, on the other hand, the sensor response on repetitive measurements of several months.

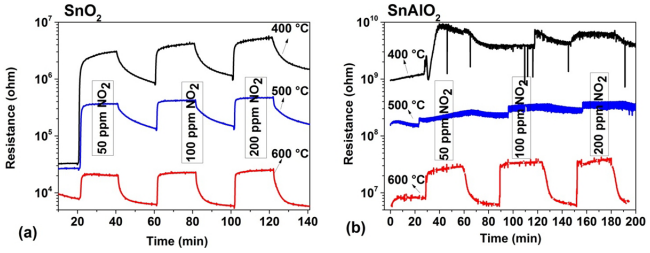

Figure 3. Dynamic responses of **(a)** SnO_2 and **(b)** SnO_2 : Al sensors when exposed to 50, 100 and 200 ppm of NO_2 gas concentrations in dry argon background, measured at $T_w = 400$, 500 and 600 °C.

3.5 Effect of background humidity and oxygen on NO_2 sensing

Several dynamic responses were recorded in order to check the effect of background humidity. A comparative plot of the two layers towards 100 ppm of NO_2 gas in 10 % RH at 500 °C is given in Fig. 4a. This plot shows that the SnO_2 : Al response to NO_2 in humidity background becomes better and stable with full baseline resistance recovery. On the other hand, in the case of undoped SnO_2 layers, the baseline is not recovered. Figure 4b shows one of the typical dynamic responses of SnO_2 : Al towards 50 ppm NO_2 in 10 % RH background for three temperatures: 400, 500 and 600 °C. The sensitivity of SnO_2 in a humidity background is highest only at 400 °C and decreases with increasing temperature and even then reaction time constants (τ_{res} and τ_{rec}) are mostly longer at 400 °C with no baseline recovery (see Table 4). On the other hand, the sensitivity of SnO_2 : Al sensors increases with increasing humidity, exhibiting a better response and recovery times at 600 °C. The response and recovery times are in the range of 1.5–5 and 6.6–20 min, respectively, in 1–10 % RH for the applied NO_2 concentrations at 400 and 500 °C. Meanwhile, the response and recovery times of SnO_2 : Al at 600 °C towards the lowest applied NO_2 concentration of 50 ppm are $\tau_{res} = 1$, 1.56 and 1.73 min and $\tau_{rec} = 7.9$, 4.8 and 2.7 min in the presence of 1, 5, and 10 % RH, respectively

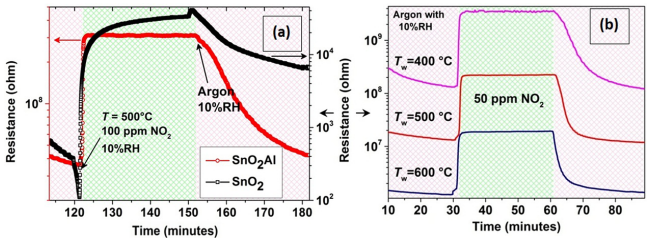

Figure 4. **(a)** Comparison of dynamic responses of SnO_2 (□) and SnO_2 : Al (◯) layers towards 100 ppm NO_2 gas in 10 % RH at 500 °C. **(b)** Typical dynamic response of the SnO_2 : Al sensor towards 50 ppm NO_2 with a cycle of 30 min switching the gas ON/OFF at $T_W = 400$, 500 and 600 °C in 10 % RH.

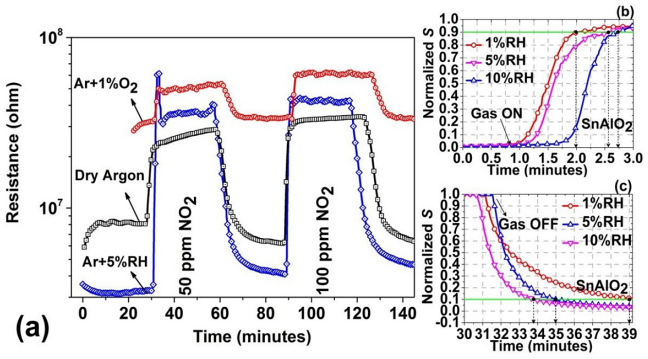

Figure 5. **(a)** The dynamic responses of SnO_2 : Al sensors when exposed to 50 and 100 ppm of NO_2 gas concentrations in dry argon, argon with 1 % oxygen and argon with 5 % RH in the background, measured at $T_W = 600$ °C. **(b)** and **(c)** provide a detailed view of the time-dependent normalized sensor response given on the right-hand side (Normalized $S = [R_{(t)} - R_{(Ar)} / R_{(NO_2)} - R_{(Ar)}]$) after the gas was switched ON and OFF. Here, $R_{(t)}$, $R_{(Ar)}$ and $R_{(NO_2)}$ denote real-time resistance, resistance in argon and NO_2 gas, respectively.

(Table 4). The procedure used for definition of the response and recovery times is presented in Fig. 5b and c. As parallel experiments confirm, in the case of oxygen background gas, the response decreases further. One of the typical responses is shown in Fig. 5a.

3.6 NO_2 cross-sensitivity

In order to check the cross-sensitivity, SnO_2 : Al sensors were tested for NO_2 and CO in combination as a single dynamic measurement towards 50 and 100 ppm gas concentrations separately and simultaneously as shown in Fig. 6. As it is demonstrated with the response curves in Fig. 6, SnO_2 : Al sensors exhibit responses to both NO_2 and CO when the gases are separately released into the test chamber. However, it is also clear that the Al-doped SnO_2 sensing layer yields a low CO cross-sensitivity when both gases are simultaneously present in the test chamber. This fact holds because the simultaneous action of NO_2 and CO yields a resistance value ($R = 5.18 \times 10^7 \Omega$; in 50 ppm NO_2+CO) near to that obtained only with NO_2 ($R = 5.5 \times 10^7 \Omega$; in 50 ppm NO_2), while the value of resistance in the presence of only 50 ppm CO is corresponding to $R = 6.49 \times 10^6 \Omega$. Meanwhile, it is observed that the baseline resistance also decreases to some extent and sensor response increases somewhat when both gases were simultaneously introduced to the SnO_2 : Al sensor ($S = 2.9$; in 50 ppm NO_2 and $S = 3.9$ in 50 ppm $NO_2 + CO$). In Sect. 4, a discussion on the possible explanation of the sensing mechanism is presented based on the results given in Sects. 3.3–3.6.

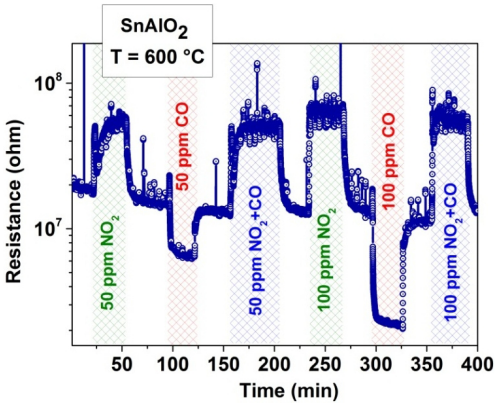

Figure 6. Dynamic response of the Al-doped SnO_2-based sensor to individual NO_2 or CO and in combination of 50 and 100 ppm of $NO_2 + CO$ gases.

4 Sensing mechanism and discussion

4.1 Humidity sensing mechanism

It is generally accepted that during heating processes, oxygen is adsorbed on the surface of metal oxides in its molecular O_2^- form ($T_W < 150$ °C) and atomic O^-/O^{2-} forms ($T_W > 150$ °C) (Zakrzewska, 2003; Haidry et al., 2012a). However, as metal-oxide sensors operate at temperatures above 150 °C, the atomic forms of oxygen are proven to influence the sensor's resistance and signal (Yamazoe and Shimanoe, 2008) according to the equation Eq. (1):

$$O_2\,(\text{gas}) + 2e^- \rightarrow 2O^-(\text{ads}). \quad (1)$$

Through adsorbed oxygen species which trap electrons and form a depletion layer, the electrical conductivity of the n-type metal-oxide layers decreases causing an upwards band bending. In case of Al doping, it is likely that the Fermi level moves towards the middle of the energy gap and ultimately creates the acceptor level (Mohagheghi and Saremi, 2004; Scanlon and Watson, 2012) below E_F similar to the case of TiO_2 (Fig. 7a). In the presence of water, H_2O can get adsorbed on the SnO_2 surface as a result of (i) a physisorption process in its molecular form at relatively lower temperatures and (ii) a chemisorption process in its ionized form at

Table 4. Comparison of response and recovery times of SnO_2 and SnO_2 : Al sensing layers towards NO_2 in the presence of 1, 5 and 10 % RH. The cells with "×" indicate incomplete baseline resistance recovery.

Humidity (%)	1 %			5 %			10 %		
NO_2 concentration (ppm)	50	100	200	50	100	200	50	100	200
SnO_2 at $T_w = 400\,°C$									
τ_{res} (min)	11	8.5	16	6.85	6.9	7.5	6.25	4.86	7.1
τ_{rec} (min)	×	×	×	9.1	×	×	21	×	×
SnO_2 : Al at $T_w = 600\,°C$									
τ_{res} (min)	1.0	1.75	2.3	1.56	2.2	2.9	1.73	1.6	3.03
τ_{rec} (min)	7.9	10.2	12.7	4.8	8.6	9.1	2.7	8.4	8.8

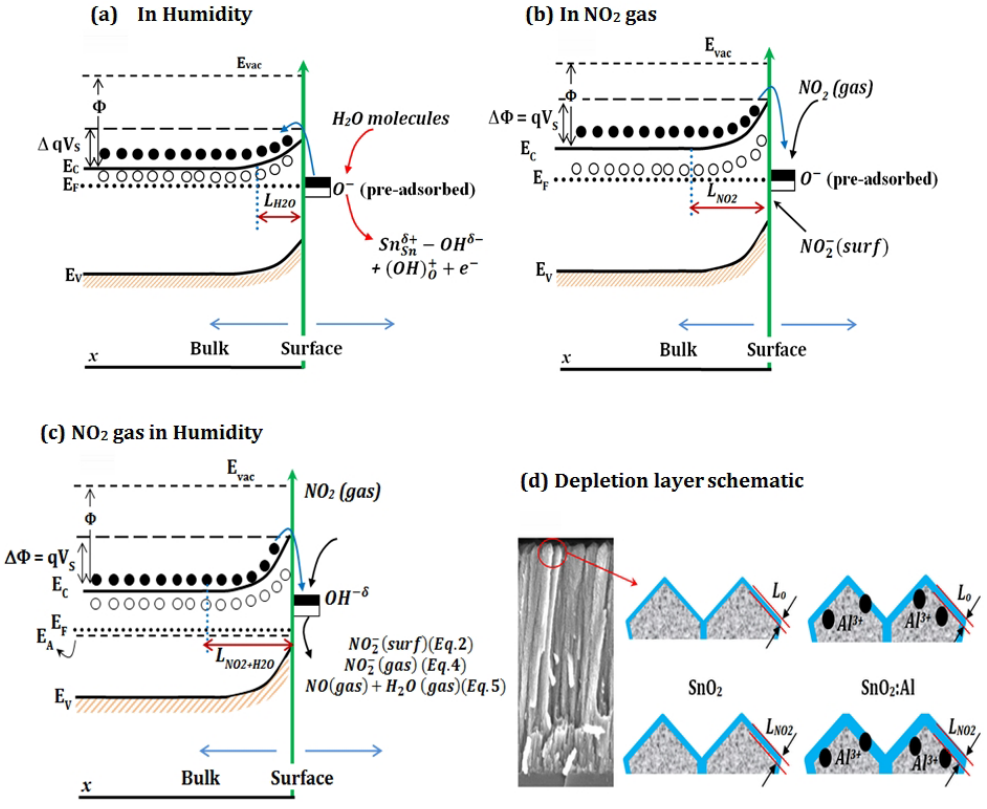

Figure 7. The illustration of the band bending due to the adsorption of oxygen species for an n-type semiconductor such as a SnO_2 layer. The schematic of chemisorption **(a)** NO_2 and **(b)** water molecules at the surface of an n-type SnO_2. **(c)** The surface reaction of SnO_2 : Al columnar structures with NO_2 under a humid environment is presented, where NO_2 reacts with pre-adsorbed $OH^{\delta-}$ groups for improved sensitivity. **(d)** The schematic of the depletion layer due to adsorption of oxygen from the environment and reaction with oxidizing gases such as NO_2; L_o and L_{NO_2} represent the depletion region on columnar morphology in argon and NO_2 environments, respectively; here $L_o < L_{NO_2}$ and $L_o(SnO_2) \ll L_o(SnO_2 : Al)$. Electrons and holes are represented by (•) and (◯), respectively.

higher temperatures. Generally, water vapors react with both surface Sn sites and surface pre-adsorbed oxygen ions. At higher temperatures e.g., above 400 °C, water molecules are adsorbed on the SnO_2 surface in the form of hydroxyl groups ($OH^{\delta-}$ groups) being active surface species and rooted OH groups (Barsan and Weimer, 2003; Cao et al., 1999). In this case, $OH^{\delta-}$ behaves like a donor on the surface (see Fig. 7a).

$$H_2O + O_O + 2Sn \leftrightarrow 2\left(Sn^{+} - OH^{-}\right) + V_O + e^{-} \quad (2)$$

The surface reaction, as described by Eq. (2), causes some release of the captured electrons back to the metal-oxide surface resulting in a decrease of the upward band bending and ultimately a decrease in the resistance (Batzill, 2006; Haidry

et al., 2012b). This is valid also for reducing gases (see e.g., Fig. 6 for CO).

4.2 NO_2 sensing mechanism

The surface reaction of oxidizing and reducing gases with undoped SnO_2-based gas sensors is well documented (Yamazoe et al., 2003, 2007; Korotcenkov, 2005); still, it is a complex mechanism, especially at higher temperatures. In this case, working temperature determines the appropriate reactions involved in sensor response as thermodynamic equilibrium of the reactive gas may deviate from the primary one. For instance, NO_2 gas transformation into a mixture of NO and NO_2 at just above 600 °C has been reported in Saruhan et al. (2013), with a fair amount of oxygen. The authors observed only NO as the temperature increased to 800 °C, while NO_2 gas was supplied in argon carrier gas. In the present case, it is believed that NO_2 is adsorbed on the SnO_2 surface as $NO^-_{2\,\mathrm{surf}}$ anions, in accordance of the following reaction in Eq. (2), as described in Cho et al. (2011):

$$NO_2\,(\mathrm{gas}) + e^- \rightarrow NO_2^-(\mathrm{surf}). \tag{3}$$

Eventually, the strong adsorption of NO_2 gas dominates over O^-/O^{2-} and creates an extended electron depletion layer ($L_o < L_{NO_2}$) leading to an increase of SnO_2 resistance (Cho et al., 2011); a schematic illustration is presented in Fig. 7b. Here, the reaction of NO_2 (gas) with pre-adsorbed oxygen O^-/O^{2-} is unlikely to occur. A superior adsorption capability of NO_2 over oxygen can also be observed in Fig. 5a, where the sensor showed a response towards NO_2 with an abundant amount of oxygen present in the background. Moreover, the response in an oxygen-rich background is lower than that in an argon background. This is also an indication that the sensing mechanism of NO_2 gas is governed by the surface adsorption of NO_2^- anions rather than the reaction through pre-adsorbed oxygen at the surface.

4.3 Effect of Al doping in the NO_2 sensing mechanism

The partial substitution of Al^{3+} in the SnO_2 lattice may result in (i) generation of more oxygen vacancies, (ii) ultimately more pre-adsorbed oxygen species, and (iii) higher resistance with $L_o(SnO_2) \ll L_o(SnO_2:Al)$ as suggested by Xu et al. (1991a) and schematically shown in Fig. 7d. This causes the different adsorption/desorption kinetics of gases on the sensor surface. In fact, the substitution of Al adds more acceptor levels resulting in lowering the Fermi level down towards center of band gap. The reaction between NO_2 and $SnO_2:Al$ surface reduces the surface electron concentration by trapping more electrons from the surface and hence an increase of resistance is noted (Sayago et al., 1995). Our results exhibit a resistance value of $SnO_2:Al$, which is about 5 orders of magnitude higher than that of pure SnO_2, i.e., $R_{SnO_2} = 2.5\times10^4\Omega \ll R_{SnO_2:Al} = 1.2\times10^9\Omega$ at 400 °C in pure argon (see Fig. 2). It has been previously reported that $SnO_2:Al$ doped with 1–5 at. % Al had a 4 order-of-magnitude higher resistance than that undoped, although further increase in the dopant level does not cause much change in the sensor resistance (in the range of a few $10^9\Omega$) (Xu et al., 1991). In addition to that, the improved sensitivity of our sensors towards NO_2 (i.e., in general towards oxidizing gases) in the presence of humidity can be explained in the light of attached surface hydroxyl groups $OH^{\delta-}$ coming from humidity. The NO_2 gas hitting the sensor surface reacts with already attached active hydroxyl groups $OH^{\delta-}$. These donors provide an increased number of adsorption sites for NO_2, thus leading to the improvement of sensor response. This explanation is valid for both sensors, undoped SnO_2 and Al-doped SnO_2. But in the case of Al-doped SnO_2 and in the presence of humidity, three possible reactions can occur simultaneously: the first is already given by Eq. (2) and the other two are expressed by Eqs. (3) and (5).

$$NO_2\,(\mathrm{gas}) + O^-\,(\mathrm{ads}) \rightarrow NO_2^-\,(\mathrm{gas}) + e^- \tag{4}$$

$$NO_2\,(\mathrm{gas}) + (M^+ - OH^-) \rightarrow NO\,(\mathrm{gas}) + H_2O(\mathrm{gas}) + MO_x + e^- \tag{5}$$

Both Eqs. (3) and (5), rely strongly on the availability of pre-adsorbed oxygen on the surface; here, M is the metal part of the reaction, in our case, that could be Sn or Al. The occurrence of the surface reactions given in Eqs. (3) and (5) is generally not possible in the case of undoped SnO_2. As a result of the reactions given in Eqs. (3) and (5), more adsorption sites on the sensor surface for NO_2 gas become available (see Fig. 7c, d). These kinds of simultaneous reactions clearly indicate the increase of sensitivity and shortening of reaction/recovery time constants for Al-doped SnO_2 sensors. It can also be noticed from our results presented in Fig. 4 that the sensor response of Al-doped SnO_2 sensors improves and becomes faster.

Low cross-sensitivity to CO in the presence of NO_2 and fast response to NO_2 achieved with an Al-doped SnO_2 sensing layer, as demonstrated in Fig. 6, can be partially associated with the Al incorporation into SnO_2. This association may be due to the doping-related electronic structure alteration (Hübner, 2011) as well as the microstructure and morphology controlled condition of the sensing layer. Al doping of SnO_2 by the sputtering process yields finer SnO_2 grains. Sintering of these fine grains, on further heat treatment of the sensing layer, results in formation of a finer crack network with higher density leading to increased grain boundary and surface area (see Figs. 1b, c and 7d). Similar observations have previously been reported in the literature (Choi et al., 2013; Liewhiran and Phanichphant, 2007; Xu at al., 1991b). As mentioned in Sect. 3.4, slower recovery and drift under dry conditions can be a result of the so-called surface poisoning effect. In the literature it is reported that the interaction of higher NO_2 concentrations with the sensor surface can cause poisoning due to the generation of doubly charged $N_2O_4^{2-}$ ions that stick to the surface of the sensor firmly and are hard

to remove. This leads to longer recovery times of the sensors at relatively low or intermediate temperatures (Ruhland et al., 1998). We assume that such poisoning may occur at lower temperatures (< 500 °C). However, this effect is eliminated as the test temperatures are increased above 500 °C and thus the sensor signal improves at 600 °C as shown in Figs. 3 and 4.

5 Conclusions

The effect of background humidity and Al doping in SnO_2 layers was investigated for the NO_2 gas response at temperatures above 400 °C. A response of similar size but in opposite direction is recorded for individual gas exposures to NO_2 and CO at 600 °C while the sensor becomes more selective towards NO_2 in a gas mixture of $CO + NO_2$. Enhanced sensitivity of SnO_2 : Al was observed towards various concentrations of NO_2 in a humid background environment, while the sensitivity is reduced in an oxygen-rich environment. The response ($\tau_{res} = 1.73$ min) and recovery ($\tau_{rec} = 2.7$ min) times towards 50 ppm NO_2 in 10 % RH are much shorter than in pure argon. The chemical stability and microstructure of SnO_2-based sensors were significantly improved by Al doping. Moreover, SnO_2 : Al layers exhibit finer grain size with a denser morphology as a result of annealing. This largely interconnected crack network leads to faster response and recovery times. In addition, the improved sensing characteristics of Al-doped SnO_2 in a humid environment were supported by the presence of hydroxyl groups, $OH^{\delta-}$, on the surface. We propose that these surface hydroxyl groups, $OH^{\delta-}$, provide more surface adsorption sites for oxidizing gas such as NO_2. Hence, these sensors would be promising candidates for monitoring NO_2 at higher temperature under humid environments with fast response rates. In addition, considering the uncomplicated processing of the material, the compatibility of thin-layer technology with modern electronics will make this sensing material more suitable for mass production.

Acknowledgements. This work has been partially supported by DAAD-DLR fellowship funding under the fellowship number 165. The authors thank Uwe Schulz, the head of the department High Temperature and Functional Coatings, for his valuable support and G. C. Mondragon Rodriguez for his assistance with FE-SEM.

Edited by: A. Lloyd Spetz
Reviewed by: three anonymous referees

References

Barsan, N., Koziej, D., and Weimer, U.: Metal oxide-based gas sensor research: How to, Sensor. Actuat. B-Chem., 121, 18–35, 2007.

Barsan, N. and Weimar, U.: Understanding the fundamental principles of metal oxide based gas sensors; The example of CO sensing with SnO_2 sensors in the presence of humidity, J. Phys. Con. Matter, 15, R813–R83, 2003.

Batzill, M.: Surface science studies of gas sensing materials: SnO_2, Sensors, 6, 1345–1366, 2006.

Batzill, M., Bergermayer, W., Tanaka, I., and Diebold, U.: Tuning the chemical functionality of a gas sensitive material: Water adsorption on SnO_2 (101), Surface Science Letters, 600, 29–32, 2006.

Bazargan, S., Thomas, J. P., and Leung, K. T.: Magnetic interaction and conical self-reorganization of aligned tin oxide nanowire array under field emission conditions, J. Appl. Phys. 113, 234305, 2013.

Bochenkov, V. E. and Sergeev, G. B.: Sensitivity, Selectivity, and Stability of Gas-Sensitive Metal-Oxide Nanostructures, in: Metal Oxide nanostructures and their applications, edited by: Ahmad, U. and Hanh, Y. B., American Scientific Publishers, 3, 31–52, 2010.

Cao, L., Spiess, F. J., Huang, A., and Suib, S. L.: Heterogeneous photocatalytic oxidation of 1-Butene on SnO_2 and TiO_2 films, J. Phys. Chem. B, 103, 2912–2917, 1999.

Chen, Z. and Lu, C.: Humidity sensors: a review of materials and mechanisms, Sens. Lett., 3, 274–295, 2005.

Cho, N. G., Yang, D. J., Jin, M. J., Kim, G. G., Tuller, H. L., and Kim, I. D.: Highly sensitive SnO_2 hollow nanofiber-based NO_2 gas sensors, Sensor. Actuat. B-Chem., 160, 1468–1472, 2011.

Choi, S.-W., Katoch, A., Sun, G.-J., Wu, P., and Kim, S. S.: NO_2-sensing performance of SnO_2 microrods by functionalization of Ag nanoparticles, J. Mater. Chem. C, 1, 2834–2841, 2013.

Faglia G., Nelli, P., and Sberveglieri, G.: Frequency effect on highly sensitive NO_2 sensors based on RGTO SnO_2(Al) thin films, Sensor. Actuat. B-Chem., 19, 497–499, 1994.

Faglia, G., Benussi, G., Depero, L., Dinelli, G., and Sberveglieri, G.: NO_2 sensing by means of SnO_2(Al) thin films grown by the rheotaxial growth and thermal oxidation technique, Sensor. Mater., 8, 239–249, 1996.

Göpel, W. and Schierbaum, K. D.: SnO_2 sensors: current status and future prospects, Sensor. Actuat. B-Chem., 26, 1–12, 1995.

Großmann, K., Wicker, S., Weimaer, U., and Barsan, N.: Impact of Pt additives on the surface reactions between SnO_2, water vapour, CO and H_2; An operando investigation, Phys. Chem. Chem. Phys., 15, 19151–19158, 2013.

Gürakar, S., Serin, T., and Serin, N.: Electrical and microstructural properties of (Cu, Al, In)-doped SnO_2 films deposited by spray pyrolysis, Adv. Mat. Lett., 5, . 309–314, 2014.

Haidry, A. A., Schlosser, P., Ďurina, P., Mikula, M., Tomášek, M., Plecenik, T. Roch, T., Pidík, A., Štefečka, M., Noskovič, J., Zahoran, M., Kúš, P., and Plecenik, A.: Hydrogen gas sensors based on nanocrystalline TiO_2 thin films, Cent. Eur. J. Phys., 9, 1351–1356, 2011.

Haidry, A. A., Puškelová, J., Plecenik, T., Ďurina, P., Greguš, J., Truchlý, M., Roch, T., Zahoran, M., Vargová, M., Kúš, P., Plecenik, A., and Plesch G.: Characterization and hydrogen gas sensing properties of TiO_2 thin films prepared by sol – gel method, Appl. Surf. Sci., 259, 270–275, 2012a.

Haidry, A. A., Ďurina, P., Tomášek, Greguš, J., Schlosser, P., Mikula, M., Truchly, M., Roch, T., Plecenik, T. Pidík, A., Zahoran, M., Kúš, P., and Plecenik, A.: Effect of post-deposition

annealing treatment on the structural, optical and gas sensing properties of TiO_2 thin films, Key Eng. Mat., 510–511, 467–474, 2012b.

Hübner, M.: New Approaches for the Basic Understanding of Semiconducting Metal Oxide Based Gas Sensors: Sensing, Transduction and Appropriate Modeling , Dissertation, Uni. Tübingen, 102–108, 2011.

Kim, B., Lu, Y., Hannon, A., Mayyappan, M., and Li, J.: Low temperature Pd/SnO_2 sensors for CO detection, Sensor. Actuat. B-Chem., 177, 770–775, 2013.

Korotcenkov, G.: Gas response control through structural and chemical modification of metal oxides: State of the art and approaches, Sensor. Actuat. B-Chem., 107, 209–232, 2005.

Korotcenkov, G., Blinov, I., Brinzari, V., and Stetter, J. R.: Effect of air humidity on gas response of SnO_2 thin films ozone sensors, Sensor. Actuat. B-Chem., 122, 519–526, 2007.

Liewhiran, C. and Phanichphant, S.: Improvement of Flame-Made ZnO nanoparticle thick film morphology for Ethanol sensing, Sensors, 7, 650–675, 2007.

Mohagheghi, M. M. B. and Saremi, M. S.: The influence of Al doping on the electrical, optical and structural properties of SnO_2 transparent conducting films deposited by the spray pyrolysis technique, J. Phys. D: Appl. Phys., 37, 1248–1253, 2004.

Pavelko, R. G., Daly, H., Hardacre, C., Vasiliev, A. A., and Llobet, E.: Interaction of water, hydrogen and their mixtures with SnO_2 based materials: the role of surface hydroxyl groups in detection mechanism, Phys. Chem. Chem. Phys., 12, 2639–2647, 2010.

Ruhland, B., Becker, T., and Müller, G.: Gas-kinetic interactions of nitrous oxides with SnO_2 surfaces, Sensor. Actuat. B-Chem., 50, 85–94, 1998.

Saruhan, B., Yüce, A., Gönüllü, Y., and Kelm, K.: Effect of Al doping on NO_2 gas sensing of TiO_2 at elevated temperatures, Sensor. Actuat. B-Chem., 187, 586–597, 2013.

Sayago, I., Gutierrez, J., Ares, L., Robla, J. I., Horrillo, M. C., Getino, J., Rino, J., and Agapito, J. A.: The effect of additives in tin oxide on the sensitivity and selectivity to NO_x and CO, Sensor. Actuat. B-Chem., 26–27, 19–23, 1995.

Scanlon, D. O. and Watson, G. W.: On the possibility of p type SnO_2, J. Mater. Chem., 22, 25236–25245, 2012.

Tricoli, A., Righettoni, M., and Teleki, A.: Semiconductor gas sensors: Dry synthesis and application, Angew. Chem. Int. Edit., 49, 7632–7659, 2010.

Xu, C., Tamaki, J., Miura, N., and Yamazoe, N.: Promotion of tin oxide gas sensor by aluminum doping, Talanta, 38, 1169–1175, 1991a.

Xu, C., Tamaki, J., Miura N., and Yamazoe, N.: Grain size effects on gas sensitivity of porous SnO_2-based elements, Sensor. Actuat. B-Chem., 3, 147–155, 1991b.

Yamazoe, N. and Shimanoe, K.: Theory of power law for metal oxide, Sensor. Actuat. B-Chem., 128, 566–573, 2008.

Yamazoe, N., Sakai, G., and Shimanoe, K.: Oxide semiconductor gas sensors, Catal. Surv. Asia, 1, 63–75, 2003.

Yamazoe, N., Shimanoe, K., and Sawada, C.: Contribution of electron tunneling transport in semiconductor gas sensors, Thin Solid Films, 515, 8302–8309, 2007.

Yamazoe, N. and Shimanoe, K.: Overview of gas sensor technology, in: Science and Technology of Chemiresistive Gas Sensors, edited by: Aswal, D. K. and Gupta, S. K., Nova Science Publisher, New York, USA, 1–32, 2007.

Zakrzewska K.: Titanium Dioxide Thin Films for Gas Sensors and Photonic Applications, AGH Ucelniane Wydawnictwa Naukowo-Dydadaktyczne, Kraków, 10–35, 2003.